



## Design of high productivity antibody capture by protein A chromatography using an integrated experimental and modeling approach

Candy K.S. Ng<sup>a</sup>, Hector Osuna-Sanchez<sup>c,1</sup>, Eric Valéry<sup>c</sup>, Eva Sørensen<sup>b</sup>, Daniel G. Bracewell<sup>a,\*</sup>

<sup>a</sup> The Advanced Centre for Biochemical Engineering, Department of Biochemical Engineering, University College London, Torrington Place, London WC1E 7JE, United Kingdom

<sup>b</sup> Centre for Process Systems Engineering, Department of Chemical Engineering, University College London, Torrington Place, London WC1E 7JE, United Kingdom

<sup>c</sup> Novasep Process, Site Eiffel – 81, Boulevard de la Moselle, BP 50, 54340 Pompey, France

### ARTICLE INFO

#### Article history:

Received 1 March 2012

Accepted 6 May 2012

Available online 14 May 2012

#### Keywords:

Protein A chromatography

Batch chromatography

Antibody capture

Productivity

Integrated process experimentation and modeling

### ABSTRACT

An integrated experimental and modeling approach for the design of high productivity protein A chromatography is presented to maximize productivity in bioprocess manufacture. The approach consists of four steps: (1) small-scale experimentation, (2) model parameter estimation, (3) productivity optimization and (4) model validation with process verification. The integrated use of process experimentation and modeling enables fewer experiments to be performed, and thus minimizes the time and materials required in order to gain process understanding, which is of key importance during process development. The application of the approach is demonstrated for the capture of antibody by a novel silica-based high performance protein A adsorbent named AbSolute. In the example, a series of pulse injections and breakthrough experiments were performed to develop a lumped parameter model, which was then used to find the best design that optimizes the productivity of a batch protein A chromatographic process for human IgG capture. An optimum productivity of  $2.9 \text{ kg L}^{-1} \text{ day}^{-1}$  for a column of 5 mm diameter and 8.5 cm length was predicted, and subsequently verified experimentally, completing the whole process design approach in only 75 person-hours (or approximately 2 weeks).

© 2012 Elsevier B.V. All rights reserved.

### 1. Introduction

Protein A chromatography is a platform technology for the capture of antibody in the biopharmaceutical industry because of its high selectivity and ease of operation afforded [1,2]. Despite these benefits, protein A chromatography is fast becoming the process bottleneck in the manufacture of antibodies due to its high associated adsorbent cost and limited capacity to handle the escalating upstream titer and market demand [3,4]. To improve this scheduling, novel protein A adsorbents with improved capacity are being proposed. However, the improved performance of these adsorbents cannot be fully exploited if the process is poorly designed, i.e. is operated at suboptimal conditions. Process optimization is therefore particularly important during the process development of protein A chromatography to ensure that the capture of antibody is both efficient and cost effective. The traditional approach to achieve this end is extensive experimentation, sometimes supported by empirical modeling or parameter estimation. Such an

approach is not only time consuming and costly, but also unlikely to find the true or global optimum.

Numerous commercially available protein A adsorbents have been studied experimentally in the literature [5–11]. These studies have improved process understanding on many aspects of the performance of protein A chromatography, such as packing quality, adsorption equilibrium and adsorption kinetics. Detailed chromatographic models, such as the ideal model [9], the surface layer model with pore diffusion [6] and the heterogeneous binding model [10], have been developed to predict breakthrough and dynamic binding capacity of protein A chromatography for the capture of antibody. These models, however, have not been employed directly for the optimal design of protein A chromatography due to their complexity. Instead analytical solutions, as used in [7,8,11], and empirical relationships, e.g. logarithmic [5] and hyperbolic [6] models, together with suitable pressure drop constraints modeled by e.g. the Blake-Kozeny equation [6] or the Carman-Kozeny equation [8,11], are applied to optimize the productivity based on a given value of breakthrough. The main drawback of such an approach is the lack of flexibility to predict and consider process yield and purity as direct constraints in the optimization problem. This is only possible if a detailed chromatography model is applied for elution as well as loading, as for instance in the process development of ion exchange and mixed-mode chromatography [12–14].

\* Corresponding author. Tel.: +44 20 7679 2374; fax: +44 20 7209 0703.

E-mail address: [d.bracewell@ucl.ac.uk](mailto:d.bracewell@ucl.ac.uk) (D.G. Bracewell).

<sup>1</sup> Present address: Processium, CEI 3 – 62, Boulevard Niels Bohr, BP 2132, F-69603 Villeurbanne Cedex, France.

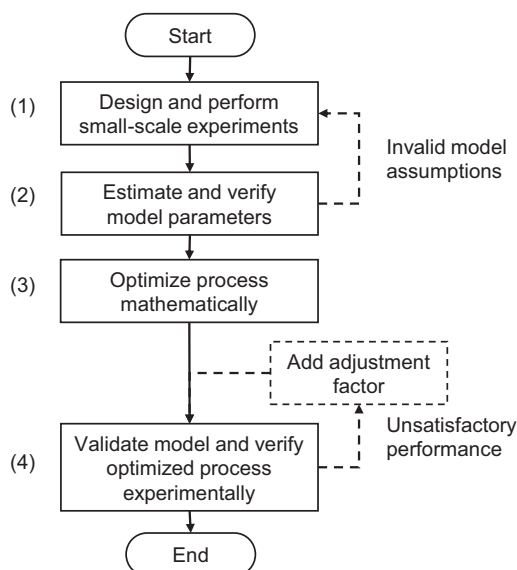


**Fig. 1.** Integrated experimental and modeling approach for optimal chromatography design.

**Table 1**  
Physical properties of AbSolute.<sup>a</sup>

Property	Units	Value
Average particle diameter, $d_p$	μm	44
Pore diameter	Å	1000
Specific surface area	m <sup>2</sup> g <sup>-1</sup>	65

<sup>a</sup> Data obtained from the manufacturer.

In the following, we demonstrate the use of an integrated experimental and modeling approach (Fig. 1) using the example of antibody capture by AbSolute, a novel silica-based high performance protein A adsorbent (Table 1). The procedure followed in this work brings together experimental protein A adsorbent characterization for model development with model-based productivity optimization. For a given process model and optimization strategy, the main steps of the approach (Fig. 1) consist of: (1) small-scale experimentation to characterize the protein A adsorbent, (2) parameter estimation based on the experimental data to determine key model parameters, (3) mathematical process optimization by applying the model developed and the chosen optimization strategy, and (4) model validation with experimental verification of the optimized process. The approach developed is general and can be applied to other chromatographic processes, e.g. ion exchange chromatography and hydrophobic interaction chromatography, and will allow quicker, less expensive and more accurate process optimization by the integration of carefully designed experiments with appropriate process modeling. Furthermore, model validation and experimental verification of the optimized process are incorporated into the approach to ensure that the model is accurate and the optimized process performance is achievable in practice. Typically model validation is performed before further applications, but here model validation was performed at the optimized batch conditions to reduce the overall experimentation efforts, and thus the time and costs, required for the approach.

## 2. Theory

For the optimal design of protein A chromatography in this work, the transport-dispersive model and an optimization strategy based on the maximization of process productivity were selected. The transport-dispersive model is a lumped parameter model that

considers diffusion, which is often the rate-limiting step in protein separation [9,12]. The mathematical model and the optimization strategy proposed in this work are summarized in Figs. 2 and 3, respectively.

### 2.1. Chromatography model

The transport-dispersive model describes the mass transfer inside the column, assuming isothermal adsorption, radial homogeneity and lumped coefficients for axial dispersion and mass transfer resistances [16]. The model comprises a mass balance for the mobile phase (Eq. (1)) and a kinetic equation for the stationary phase adsorption (Eq. (2)):

$$\frac{\partial C}{\partial t} + \frac{1 - \varepsilon_T}{\varepsilon_T} \frac{\partial q}{\partial t} + \frac{u}{\varepsilon_T} \frac{\partial C}{\partial z} = D_L \frac{\partial^2 C}{\partial z^2} \quad (1)$$

$$\frac{\partial q}{\partial t} = k_m(q^* - q) \quad (2)$$

where  $C$  and  $q$  are the solute concentrations in the mobile and stationary phases, respectively,  $t$  is the time coordinate,  $z$  is the axial coordinate,  $\varepsilon_T$  is the total porosity,  $u$  is the superficial velocity,  $D_L$  is the apparent axial dispersion coefficient,  $k_m$  is the lumped mass transfer coefficient, and  $q^*$  is the solute concentration in the stationary phase at equilibrium as defined by the adsorption equilibrium isotherm. The driving force in Eq. (2) [16] distinguishes the transport-dispersive model from the equilibrium-dispersive model, which assumes instantaneous equilibrium between the mobile and stationary phases (i.e.  $q = q^*$ ).

The apparent axial dispersion coefficient,  $D_L$ , is in this work defined by an empirical correlation [16]:

$$D_L = \frac{uL}{2N} \quad (3)$$

where  $N$  is the theoretical plate number as correlated to the linear velocity,  $u$ , by Eq. (4) [16] and the modified van Deemter expression in Eq. (5) [17]:

$$h = \frac{L}{Nd_p} \quad (4)$$

$$h = A + Bu \quad (5)$$

where  $h$  is the reduced plate height,  $d_p$  is the particle diameter, and  $A$  and  $B$  are the van Deemter coefficients for the eddy diffusion and the mass transfer resistances, respectively. The two terms in Eq. (5) were assumed to be additive despite their different dependences on the linear velocity. Longitudinal diffusion was assumed to be negligible.

The lumped mass transfer coefficient,  $k_m$ , in the transport-dispersive model (Eq. (2)) was assumed to be a variable following the empirical correlation proposed in Eq. (6):

$$k_m = k_{\max} \left[ S_1 + (1 - S_1) \left( 1 - \frac{q_R}{q_{\max,R}} \right)^{S_2} \right], \quad \text{where } 0 \leq S_1 \leq 1 \text{ and } S_2 > 0 \quad (6)$$

$k_{\max}$  is the maximum lumped mass transfer coefficient,  $q_R$  is the sum of all the retained solute concentrations in the stationary phase,  $q_{\max,R}$  is the maximum binding capacity of all the retained solutes from the adsorption equilibrium isotherm, and  $S_1$  and  $S_2$  are the saturation dependent kinetic constant and order, respectively.

The column is assumed to be initially empty of solutes in both the mobile and stationary phases. At the column inlet, the axial concentration change depends on the difference between the feed and column inlet concentrations. At the column outlet, it is assumed that there is no axial concentration change. These initial and Danckwerts's boundary conditions are given in Eqs. (7)–(10) [18]:

$$C(t = 0, z) = 0 \quad (7)$$

$$q(t = 0, z) = 0 \quad (8)$$

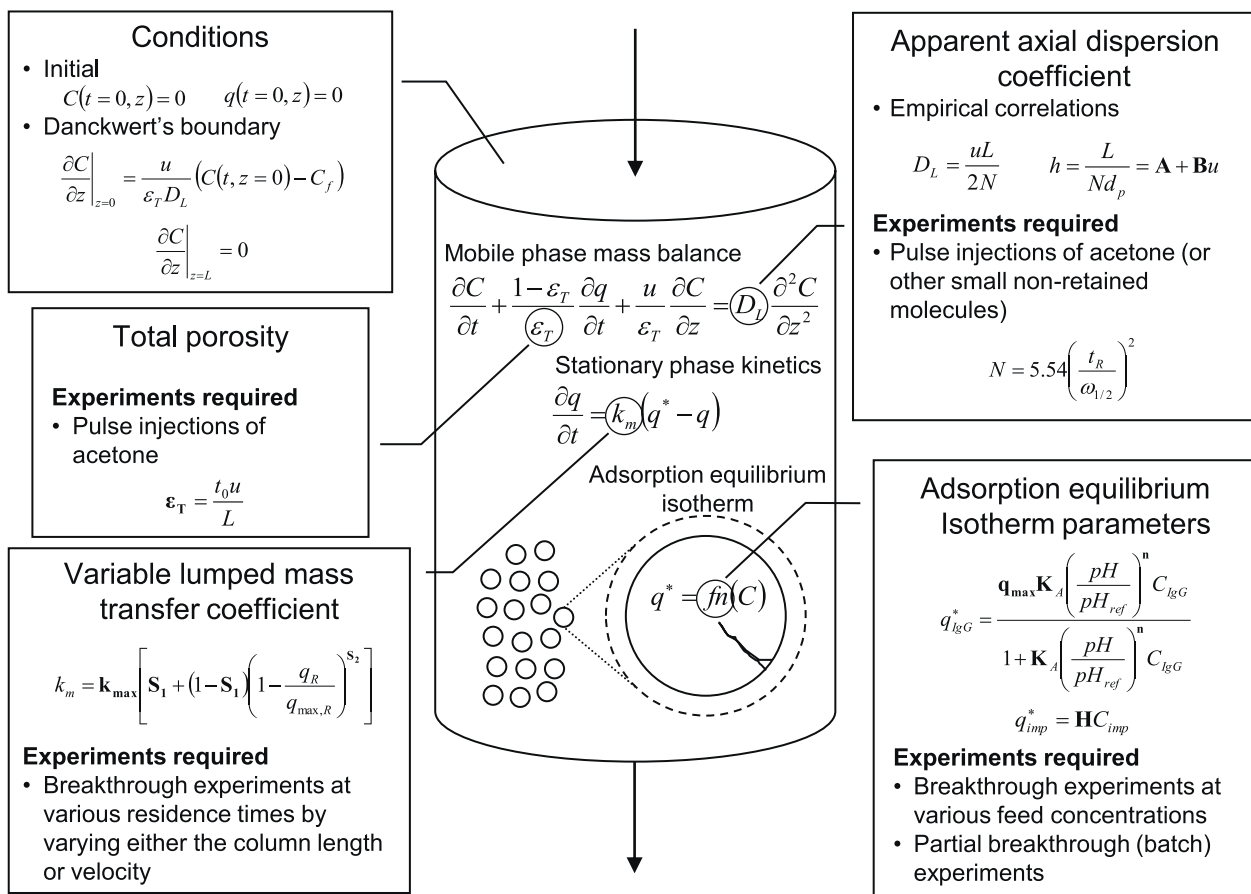


Fig. 2. Modeling strategy indicating experiments required for modified transport-dispersive model development.

$$\left. \frac{\partial C}{\partial z} \right|_{z=0} = \frac{u}{\varepsilon_T D_L} (C(t, z=0) - C_f), \quad \text{where } C_f \neq 0 \text{ for } 0 < t < t_L \quad (9)$$

$$\left. \frac{\partial C}{\partial z} \right|_{z=L} = 0 \quad (10)$$

Different adsorption isotherms can be used in this approach. For the process example considered in this work of IgG capture by protein A chromatography, the components involved were assumed to behave as two pseudo-components: IgG and impurities. Here, IgG is the product and refers to all the retained materials during pulse injections under loading conditions, whereas impurities refer to all the non-retained materials under the same conditions. For IgG, a Langmuir adsorption isotherm considering pH as a modifier [19] (Eq. (11)) was selected. The impurities were assumed to follow a linear adsorption isotherm (Eq. (12)) [16].

$$q_{lgG}^* = \frac{q_{\max} K_A (\text{pH}/\text{pH}_{ref})^n C_{lgG}}{1 + K_A (\text{pH}/\text{pH}_{ref})^n C_{lgG}} \quad (11)$$

$$q_{imp}^* = HC_{imp} \quad (12)$$

$C_{lgG}$  is the IgG concentration in the mobile phase,  $q_{lgG}^*$  is the IgG concentration in the stationary phase at equilibrium,  $q_{\max}$  is the maximum binding capacity,  $K_A$  is the association equilibrium constant,  $\text{pH}_{ref}$  is the reference pH (in this work, of the loading zone),  $n$  is the pH dependent equilibrium order,  $C_{imp}$  is the impurity concentration in the mobile phase,  $q_{imp}^*$  is the impurity concentration

in the stationary phase at equilibrium, and  $H$  is the linear isotherm constant.

In total, there were ten parameters in the selected transport-dispersive model (in bold in Fig. 2) which needed to be estimated:  $\varepsilon_T$  in Eq. (1),  $A$  and  $B$  in Eq. (5),  $k_{\max}$ ,  $S_1$  and  $S_2$  in Eq. (6),  $q_{\max}$ ,  $K_A$  and  $n$  in Eq. (11), and  $H$  in Eq. (12). The model, consisting of Eqs. (1)–(6) and Eqs. (11) and (12) with initial and boundary conditions given by Eqs. (7)–(10), was discretized by orthogonal collocation

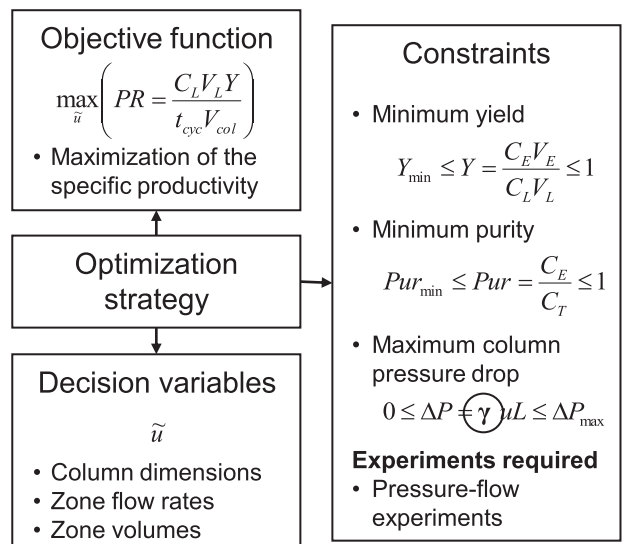


Fig. 3. Productivity optimization strategy indicating experiments required.

on finite elements [20,21] and solved in C++ using the implicit differential-algebraic (IDA) solver in the suite of nonlinear and differential/algebraic equation solvers (SUNDIALS) [22].

## 2.2. Optimization strategy

The objective function considered in this work is to maximize the productivity,  $PR$ , (Eq. (13)) subject to the constraints given by Eqs. (14)–(16):

$$\max_{\tilde{u}} PR \quad (13)$$

$$Y_{\min} \leq Y \leq 1 \quad (14)$$

$$Pur_{\min} \leq Pur \leq 1 \quad (15)$$

$$0 \leq \Delta P \leq \Delta P_{\max} \quad (16)$$

where  $\tilde{u}$  is the vector containing the decision variables (in this work, column length, flow rates and volumes for load, wash, elution, regeneration and equilibration) to be determined by the optimizer,  $Y$  is the product yield,  $Pur$  is the product purity, and  $\Delta P$  is the column pressure drop.

Productivity, yield, purity and column pressure drop are defined as follows:

$$PR = \frac{C_L V_L Y}{t_{cyc} V_{col}} \quad (17)$$

$$Y = \frac{C_E V_E}{C_L V_L} \quad (18)$$

$$Pur = \frac{C_E}{C_T} \quad (19)$$

$$\frac{\Delta P}{L} = \gamma u \quad (20)$$

where  $C_L$ ,  $C_E$  and  $C_T$  are the loaded product, eluted product and total eluted concentrations,  $V_L$  and  $V_E$  are the load and elution volumes,  $t_{cyc}$  is the cycle time,  $V_{col}$  is the column volume,  $L$  is the column length,  $\gamma$  is the apparent friction factor that needs to be fitted experimentally (Fig. 3), and  $u$  is the linear velocity of the mobile phase in the column.

Productivity,  $PR$ , (defined in Eq. (17)) was used as the objective function for optimization as it provides a reasonable indication of process economics and detailed cost data is often not available. Since protein A adsorbents are expensive and contribute significantly towards the total process costs, the process with the maximum productivity requires the least amount of adsorbents to process a given batch, which corresponds to the lowest adsorbent costs, and thus implies the best process economics. Throughput,  $Thr = PR V_{col}$ , is another process attribute and is related to the optimized productivity,  $PR$ , through the column volume,  $V_{col}$ . Yield,  $Y$ , (Eq. (18)) is important because protein A chromatography capture is normally the first purification step and therefore influences the overall product recovery in bioprocess manufacture. Purity,  $Pur$ , (Eq. (19)) is concerned with product quality and also affects the subsequent manufacturing steps. Column pressure drop,  $\Delta P$ , (Eq. (20)) is an operational constraint for practical process applications and cannot exceed a maximum value for safety reasons.

In this work, the optimization problem consisting of Eqs. (13)–(20), and based on the selected transport-dispersive model described earlier, was solved in Delphi 7 using constrained optimization by linear approximation [23], which is a sequential trusted-region algorithm that maintains a regular-shaped simplex over the iterations by linear approximations of the objective function and constraints.

## 3. Materials and methods

The experimental details described below are for the process example based on a novel silica-based high performance protein A adsorbent called AbSolute. Three types of experiment were performed for parameter estimations as outlined in the following.

### 3.1. Materials

All components except those listed below were obtained from Sigma-Aldrich Chimie SARL (Lyon, France). The protein A adsorbent AbSolute was obtained from Novasep Process (Pompey, France). The feed used was a mixture of human IgG and bovine serum. Human polyclonal IgG in the form of lyophilized powder was obtained from Equitech Bio, Inc. (Kerrville, Texas, US) and bovine serum was obtained from Eurobio (Courtaboeuf, France). Glycine, sodium chloride and disodium phosphate were obtained from Merck Santé SAS (Lyon, France), hydrochloric acid was obtained from Fisher Scientific Labosi (Elancourt, France), and glacial acetic acid, phosphoric acid and acetonitrile were obtained from Carlo Erba Reactifs (Val de Reuil, France).

VacuCap 90 PF filter units were obtained from Pall Life Sciences (Saint-Germain-en-Laye, France). Tricorn 5/50 columns were obtained from GE Healthcare (Uppsala, Sweden). A Poros A 20 pre-packed column (4.6/50) was obtained from Life Technologies (Cergy-Pontoise, France) for protein A high performance liquid chromatography (HPLC).

The experimental setup comprises a typical HPLC system: an Alliance HPLC Bio System bioseparations module (2796) with multiple inlets, pumps, a pressure detector, an autosampler, an injection system and a column holder, together with a photodiode array detector (2996) of path length 1.0 cm from Waters SAS (Saint-Quentin En Yvelines, France) and a combined module of pH and conductivity detectors (pH/C-900) from GE Healthcare (Uppsala, Sweden) at the column outlet. The HPLC system was used for both the small-scale experiments and the HPLC assays for IgG yield and purity [5,24]. The combined module of pH and conductivity detectors was optional but useful in monitoring protein A chromatography, the zones (i.e. loading, wash, elution, regeneration and equilibration) of which are principally characterized by pH.

### 3.2. Pressure-flow and pulse injection experiments

Pressure-flow and pulse injection experiments were performed to determine the hydrodynamics of AbSolute (total porosity,  $\varepsilon_T$ , in Eq. (1), van Deemter coefficients,  $A$  and  $B$ , in Eq. (5), and apparent friction factor,  $\gamma$ , in Eq. (20)).

Pulses of acetone (10  $\mu$ L) were injected into the system with and without the column at linear velocities,  $u$ , of 100, 150, 300, 600 and 1500  $\text{cm h}^{-1}$  with water as the mobile phase to determine the total porosity ( $\varepsilon_T$  in Eq. (1)) and the van Deemter coefficients ( $A$  and  $B$  in Eq. (5)). The peaks were measured at the column outlet by absorbance at 280 nm.

A pressure-flow curve of AbSolute was obtained from the manufacturer to determine the apparent friction factor ( $\gamma$  in Eq. (20)). Column pressure drops (the differences between the system pressures with and without the column) were measured for a column of 5 mm diameter and 20 cm length,  $L$ , using phosphate buffered saline (PBS), pH 7.4, at linear velocities,  $u$ , of 60, 120, 150, 240, 300, 450, 600, 750 and 900  $\text{cm h}^{-1}$ .

### 3.3. Breakthrough experiments

Three sets of breakthrough experiments were performed in small-scale Tricorn columns of 5 mm diameter and 5 cm length at conditions listed in Table 2 to determine the adsorption properties

**Table 2**  
Breakthrough experimental conditions.

Experimental condition	Set 1	Set 2	Set 3
Human IgG concentration ( $\text{g L}^{-1}$ )	1, 2, 5, 10	1	1
Linear velocity ( $\text{cm h}^{-1}$ )	300	100, 300, 600, 1500	200, 600
Equilibration (CV)	5	5	5
Load (CV)	200	200	40, 30
Wash (CV)	10	10	3
Elution (CV)	5	5	5
Regeneration (CV)	5	5	4
Equilibration (CV)	5	5	4

of AbSolute ( $k_{\max}$ ,  $S_1$  and  $S_2$  in Eq. (6),  $q_{\max}$ ,  $K_A$  and  $n$  in Eq. (11), and  $H$  in Eq. (12)). PBS, pH 7.4, was used for equilibration and wash. 0.1 M glycine-HCl, pH 3, and HCl, pH 1.5, were used for elution and regeneration, respectively. All buffers were degassed by sonication prior to use. The feed containing dissolved human IgG, bovine serum or both in PBS, pH 7.4, was filtered at 0.8/0.2  $\mu\text{m}$  using VacuCap 90 PF filter units to remove undissolved particulates and kept in an ice bath. Solute concentrations were measured at the column outlet by absorbance at 280 nm, or 300 nm in the case of signal saturation at 280 nm, for which linear IgG calibration curves were observed (data not shown).

### 3.4. Assay

Protein A HPLC was used to determine the experimental performance (yield,  $Y$ , in Eq. (18) and purity,  $Pur$ , in Eq. (19)) of the optimized batch by measuring IgG concentrations in the feed and the various pools (flowthrough, wash, eluate, regenerate and equilibration). Each analysis took 4.5 min using a Poros A 20 pre-packed protein A analytical column of 4.6 mm diameter and 5 cm length with 20  $\mu\text{m}$  particles. Samples of 30  $\mu\text{l}$  were injected at 2  $\text{ml min}^{-1}$  and peak areas were measured at 280 nm. After injection, the column was washed with buffer A (100 mM sodium phosphate, 250 mM sodium chloride, pH 6.3) for 1 min. Bound IgG was eluted by a gradient of 100% buffer A to 100% buffer B (2% acetic acid, 10 mM glycine, pH 2.5) over 1 min. After the hold at 100% buffer B for 0.5 min, the column was regenerated with buffer C (0.1% phosphoric acid, 20% acetonitrile) for 1 min before equilibrating with buffer A for 1 min.

## 4. Results and discussion

The results obtained for the process example on AbSolute following the integrated approach in Fig. 1 are organized as followed: experimental results and parameter estimations (steps 1 and 2); model-based process productivity optimization (step 3); and model validation with optimized process verification (step 4).

### 4.1. Experimental results and parameter estimations

Experimentation is essential for proper model development to gain better understanding of the chromatographic process performance and to estimate accurate model parameters. By selecting a lumped parameter model, as opposed to a general rate model, the number of key model parameters to be estimated, and thus the experimentation effort for parameter estimation, can be drastically reduced whilst still ensuring sufficient model accuracy [15].

In total, 11 parameters were identified from the proposed process model and optimization strategy (Figs. 2 and 3). A series of carefully designed experiments were therefore performed at small scale to minimize the resources required to obtain these model parameters (step 1 in Fig. 1). The experimental results for AbSolute, along with the estimation of the key model parameters (step 2 in

Fig. 1), will be presented next and discussed as follows: total porosity, axial dispersion and friction, adsorption equilibrium, and mass transfer. The estimated model parameters and the corresponding experiments are summarized in Table 3. Errors in the estimated model parameters were determined statistically and are only available for the parameters estimated by a least squares' method.

#### 4.1.1. Total porosity, axial dispersion and friction

The total porosity,  $\varepsilon_T$ , was estimated from the pulse injection experiments using Eq. (21) [16]:

$$\varepsilon_T = \frac{t_0 u}{L} \quad (21)$$

where  $t_0$  is the column dead time that was calculated as the difference between the retention times from pulse injections into the system with and without column, and  $L$  is the column length. The estimated value of the total porosity was the average value obtained at three flow rates. A total porosity ( $\varepsilon_T$ ) of approximately  $0.8 \pm 0.1$  was estimated for AbSolute. The data at  $1500 \text{ cm h}^{-1}$  was omitted due to the high error associated with retention times of less than 1 s.

The peaks that were obtained from the pulse injection experiments with the column were used to calculate the reduced plate height,  $h$ , using Eqs. (4) and (22) [15]:

$$N = 5.54 \left( \frac{t_R}{\omega_{1/2}} \right)^2 \quad (22)$$

where  $t_R$  is the retention time, which requires extra-column corrections except if the extra-column volume is less than 10% of the peak volume [25], and  $\omega_{1/2}$  is the peak width at half maximum peak height. The van Deemter coefficients ( $A$  and  $B$ ) were then estimated by linearly fitting the reduced plate height,  $h$ , versus the linear velocity of the mobile phase,  $u$ , using Eq. (5), as shown in Fig. 4A.

For the equipment used, extra-column contribution to the van Deemter coefficients was negligible considering the peak volume and the extra-column volume that were determined by pulse injections into the system with and without the column, respectively. The van Deemter coefficients for the eddy diffusion and the mass transfer resistances of AbSolute ( $A$  and  $B$ ) were estimated to be  $4.8 \pm 0.1$  and  $17 \pm 1 \text{ s cm}^{-1}$ , respectively. The small errors of these fitted parameters and the high correlation coefficient of 0.996 for Fig. 4A indicate that longitudinal diffusion is negligible for AbSolute at flows greater than  $100 \text{ cm h}^{-1}$ .

The apparent friction factor,  $\gamma$ , is necessary for the optimization to ensure that the column pressure drop constraint is satisfied at all times. The value of the apparent friction factor,  $\gamma$ , was estimated from the pressure-flow experiments by linearly fitting the normalized column pressure drop,  $\Delta P/L$ , against the linear velocity of the mobile phase,  $u$ , using Eq. (20), as illustrated in Fig. 4B. Only data in the linear pressure-flow region, where columns are generally operated, were fitted. A minimum of two, and preferably five, pressure-flow data in the linear region is required. In Fig. 4B, linear pressure-flow was observed for AbSolute at linear velocities up to  $1000 \text{ cm h}^{-1}$ . This confirms that AbSolute is rigid and incompressible, as only shorter linear pressure-flow ranges up to  $600 \text{ cm h}^{-1}$  have previously been reported for compressible matrices [8,11,26]. The apparent friction factor,  $\gamma$ , for AbSolute was estimated to be  $(1.25 \pm 0.01) \times 10^{-4} \text{ bar h cm}^{-2}$ . This estimated value is in the same order of magnitude as that reported for Prosep-vA Ultra ( $0.4 \times 10^{-4} \text{ bar h cm}^{-2}$ ), another silica-based protein A adsorbent, by McCue et al. [6] when considering the difference in the average particle sizes (44  $\mu\text{m}$  for AbSolute versus 100  $\mu\text{m}$  for Prosep-vA Ultra).

**Table 3**

Estimated model parameters from experimental data for AbSolute.

Parameter	Symbol	Experiment	Eq.	Units	Value <sup>a</sup>
Total porosity	$\varepsilon_T$	Pulse injection	(1)		$0.8 \pm 0.1$
van Deemter eddy diffusion coefficient	$A$	Pulse injection	(5)		$4.8 \pm 0.1$
van Deemter mass transfer resistances coefficient	$B$	Pulse injection	(5)	$\text{s cm}^{-1}$	$17 \pm 1$
Apparent friction factor	$\gamma$	Pressure-flow	(20)	$\text{bar h cm}^{-2}$	$(1.25 \pm 0.01) \times 10^{-4}$
Maximum binding capacity	$q_{\max}$	Breakthrough <sup>b</sup>	(11)	$\text{g L}^{-1}$	$73 \pm 3$
Association equilibrium constant	$K_A$	Breakthrough <sup>b</sup>	(11)	$\text{L g}^{-1}$	$6.1 \pm 2.9$
Linear isotherm constant	$H$	Breakthrough <sup>b</sup>	(12)		$1.6 \pm 0.0$
Maximum lumped mass transfer coefficient	$k_{\max}$	Breakthrough <sup>c</sup>	(6)	$\text{s}^{-1}$	1.6
Saturation dependent kinetic constant	$S_1$	Breakthrough <sup>c</sup>	(6)		0.26
Saturation dependent kinetic order	$S_2$	Breakthrough <sup>c</sup>	(6)		4.0
pH dependent equilibrium order	$n$	Breakthrough <sup>d</sup>	(11)		16.6

<sup>a</sup> Errors where given are  $\pm 1$  standard deviation.<sup>b</sup> Breakthrough at various concentrations.<sup>c</sup> Breakthrough at various residence times.<sup>d</sup> Partial breakthroughs at various residence times.

#### 4.1.2. Adsorption equilibrium

An adsorption equilibrium isotherm describes the solute concentration in the stationary phase at equilibrium (or equilibrium binding capacities,  $q^*$ ) as a function of the solute concentration in the mobile phase ( $C$ ). The column uptake approach based on breakthrough experiments was selected for the measurement of the equilibrium binding capacities to avoid the need for additional experimental setup in batch stirred tanks and further errors from the measurement of the amount of adsorbent. Hence such a column uptake approach is generally more accurate than a batch stirred tank uptake approach [27]. The equilibrium binding capacities of

the solute were estimated by area integration of the breakthrough curves [8], rather than by interpolation of the breakthrough curves at 50% breakthrough [5,7], to obtain more realistic estimates as breakthrough curves for protein A adsorbents are typically asymmetric [5–10]. Area integration of the breakthrough curves was approximated by the trapezium rule. The equilibrium binding capacity data was then fitted to Eqs. (11) and (12) to estimate the isotherm constants ( $q_{\max}$  and  $K_A$  in Eq. (11) and  $H$  in Eq. (12)).

The Langmuir adsorption isotherm (Eq. (11)) was used because it is the most commonly used representation of the non-linear adsorption equilibrium for protein A chromatography [6–10]. The consideration of pH as a modifier [19] enabled the IgG adsorption equilibrium under various pHs to be described with only one additional parameter. The impurities were assumed to follow a linear adsorption isotherm (Eq. (12)) for model simplicity and to ease experimentation for parameter estimation.

In the example, two plateaus were expected in the absorbance signal during the loading of AbSolute, due to the flowthrough of human IgG3, IgG-unrelated materials, or both (Fig. 5). These non-retained materials were regarded as impurities, and thus the first, earlier plateau (10% of the feed concentration) was used to estimate the linear isotherm constant,  $H$  in Eq. (12), and the second, later plateau (90% of the feed concentration) was considered to estimate the Langmuir isotherm constants,  $q_{\max}$  and  $K_A$  in Eq. (11). The effect of pH on the IgG adsorption equilibrium, i.e.  $n$  in Eq. (11), was determined later using the desorption curves during elution in the third set of the breakthrough experiments.

For AbSolute, the equilibrium binding capacities of IgG and the impurities were estimated from the first set of the breakthrough experiments (Table 2). A linear velocity of  $300 \text{ cm h}^{-1}$  was selected to minimize the experimental time without significantly compromising the breakthrough curve accuracy. A load of  $200 \text{ g(L bed)}^{-1}$  was used to obtain breakthrough over 90%. The experimental concentration range for isotherm determination should be as wide as possible to obtain accurate isotherm parameters [28]. The standard deviation for the estimated IgG equilibrium binding capacities ( $q_{\text{IgG}}^*$ ), based on breakthrough at the same conditions but using two individual columns, was less than  $0.01 \text{ g L}^{-1}$ . A maximum binding capacity,  $q_{\max}$ , of  $73 \pm 3 \text{ g L}^{-1}$  and an association equilibrium constant,  $K_A$ , of  $6.1 \pm 2.9 \text{ L g}^{-1}$  were obtained for IgG adsorption up to  $9 \text{ g L}^{-1}$  by AbSolute. It should be noted that the estimated maximum binding capacity of  $73 \text{ g L}^{-1}$  for AbSolute is higher than those previously reported in the literature for IgG adsorption, which generally fall within  $37$ – $69 \text{ g L}^{-1}$  [6–8,10]. This may be related to the large specific surface area of AbSolute particles ( $65 \text{ m}^2 \text{ g}^{-1}$ ) for ligand coupling. The association equilibrium constant for AbSolute is in the low range of those found for other protein A adsorbents, which is around  $3.2$ – $72 \text{ L g}^{-1}$  [6–8,10]. This can be explained by the

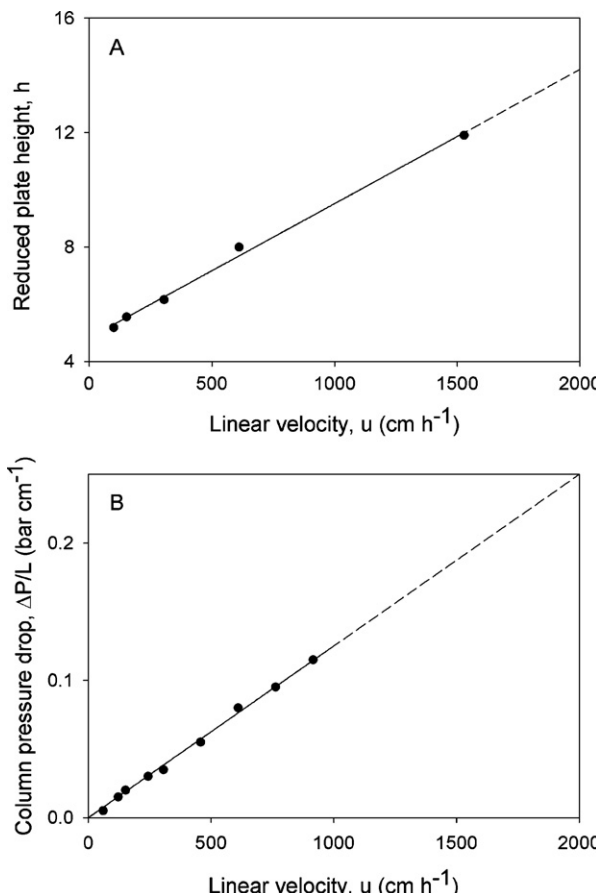


**Fig. 4.** (A) Column efficiency-flow curve for AbSolute using a column of  $5 \text{ mm } D \times 50 \text{ mm } L$  with water as mobile phase with a  $R^2$  of 0.996. (B) Pressure-flow curve for AbSolute using a column of  $5 \text{ mm } D \times 200 \text{ mm } L$  with PBS, pH 7.4, as mobile phase with a  $R^2$  of 0.997 (courtesy of Novasep).

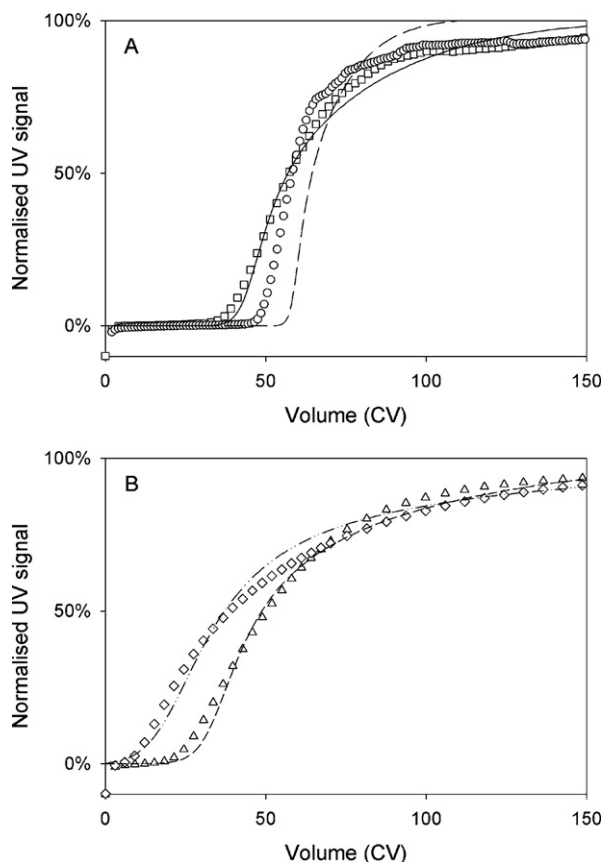


**Fig. 5.** Experimental (dotted) and fitted (dashed) breakthrough curves of  $0.9 \text{ g L}^{-1}$  IgG for AbSolute using a column of  $5 \text{ mm } D \times 50 \text{ mm } L$  with PBS, pH 7.4, as mobile phase flowing at (A: ○, - -)  $100 \text{ cm h}^{-1}$ , (A: □, - -)  $300 \text{ cm h}^{-1}$ , (B: △, - -)  $600 \text{ cm h}^{-1}$  and (B: ◇, - -)  $1000 \text{ cm h}^{-1}$ , measured at an absorbance of  $280 \text{ nm}$ .

experimental data range used to estimate the isotherm, the lowest IgG concentration being  $0.9 \text{ g L}^{-1}$  for practical reasons and to be in keeping with the working range for the simulations. Therefore any uncertainty in the association equilibrium constant would not have a significant impact in the operating ranges of interest. A linear isotherm constant,  $H$ , of  $1.6 \pm 0.0$  was estimated for the adsorption of impurities up to  $0.9 \text{ g L}^{-1}$  by AbSolute.

#### 4.1.3. Mass transfer

The lumped mass transfer coefficient,  $k_m$ , in the transport-dispersive model (Eq. (2)) is typically assumed to be a constant. This, however, is not appropriate when the breakthrough curves are asymmetric. Consequently, we introduced a variable lumped mass transfer coefficient (Eq. (6)) where the effects of adsorption on kinetic limitations were considered empirically using a power law based on the fraction of free sites available,  $1 - q_R/q_{\max,R}$ . The use of Eq. (6) enables more accurate breakthrough predictions in the absence of a complex model (such as the surface layer model with pore diffusion [6] and the heterogeneous binding model [10]). Adsorption kinetics was assumed to be the same for both IgG and the impurities as the impurities consist of a range of solutes that include non-retainable IgG.

The kinetic parameters ( $k_{\max}$ ,  $S_1$  and  $S_2$  in Eq. (6)) were estimated simultaneously from the second set of the breakthrough experiments (Table 2) by fitting the breakthrough curves at various linear velocities,  $u$ , to the whole model with the other parameters fitted so far using constrained optimization by linear approximation [23] to minimize the error between the experimental and simulated curves, see the example shown in Fig. 5. Constrained optimization by linear approximation was used because this

algorithm is derivative-free, and thus easier to use than gradient-based algorithms. The concentration of human IgG for this set of breakthrough experiments was selected such that it is similar to that used for optimization later. The model without the pH dependent Eq. (11) (i.e.  $q_{\text{IgG}}^* = q_{\max} K_A C_{\text{IgG}} / (1 + K_A C_{\text{IgG}})$ ) was sufficient for fitting the breakthrough curves at the reference pH,  $\text{pH}_{\text{ref}}$ .

For AbSolute, the maximum lumped mass transfer coefficient,  $k_{\max}$ , saturation dependent kinetic constant,  $S_1$ , and order,  $S_2$ , were estimated to be  $1.6 \text{ s}^{-1}$ , 0.26 and 4.0, respectively. The determination of these kinetic parameters required a total of 42 min CPU time on two Intel Xeon E5520 processors of  $2.26 \text{ GHz}$  with  $24.0 \text{ Gb}$  memory. The fitted breakthrough curves in Fig. 5 deviate somewhat from the experimental curves that were overlaid together, especially for the breakthrough at  $100 \text{ cm h}^{-1}$ . This suggests that the fitted kinetic parameters are inappropriate for the prediction of breakthrough behavior at flow rates below  $300 \text{ cm h}^{-1}$ . Packed bed behavior towards equilibrium, i.e. for breakthrough above 60%, was poorly fitted, as expected from the use of a lumped parameter model instead of a more complex, general rate model. However, only the early breakthrough behavior is important for the design of a batch process, where breakthrough of 10% or lower is usually applied [5,6,11].

As reported for almost all protein A adsorbents [8,10], difficulties in reaching complete column saturation are observed as can be seen in Fig. 5. High flow rate IgG breakthrough curves are asymmetric as can be clearly seen in Fig. 5B. Possible causes for these observations have been suggested and include molecular stretching and changes in transport mechanism upon adsorption [8]. Other effects include broad particle size distribution, competition between monomers and aggregates, and the polyclonal nature of the IgG used. These factors were not assumed to have had any effect as AbSolute has a very narrow particle size distribution and furthermore the same behavior as that seen in Fig. 5 was also observed by Perez-Almodovar and Carta [10] for the breakthrough of purified monoclonal antibody without aggregates. Hence, the main cause for the incomplete and asymmetric saturation is therefore likely to be kinetic limitations that are adsorption related.

One final parameter needed to be fitted: the pH dependent equilibrium order,  $n$ , in Eq. (11), which predicts the IgG adsorption equilibrium at low pH. This parameter,  $n$ , must be estimated from the third set of the breakthrough experiments (Table 2) after the determination of kinetic parameters. This is because the desorption curves observed during elution are dynamic and generally saturated, and thus the estimated amount of IgG desorbed during elution, which provides an estimate of the IgG adsorption equilibrium at low pH, depends on mass transfer inside the column given by the kinetic parameters. Again, the error between the experimental and simulated curves was minimized using constrained optimization by linear approximation [23].

Fig. 6 shows the chromatograms that were obtained from the partial breakthrough (or batch) runs. Only the unsaturated experimental signal, i.e. within 2 AU at  $280 \text{ nm}$ , was considered for parameter fitting due to the unreliability of the saturated signal. Since simulation is not limited by signal saturation, the simulated elution curves provide more reliable projections of IgG desorption at low pH than the experimental elution curves (Fig. 6). The pH dependent equilibrium order,  $n$ , for AbSolute was estimated to be 16.6. This value confirms that IgG adsorption by AbSolute is drastically reduced with decreasing pH, as expected.

#### 4.1.4. Performance of lumped parameter model

A lumped chromatography model has been presented above which predicts IgG adsorption by AbSolute based on a combination of empirical correlations and curve fitting of the experimental results. Table 3 summarizes the estimated model parameters

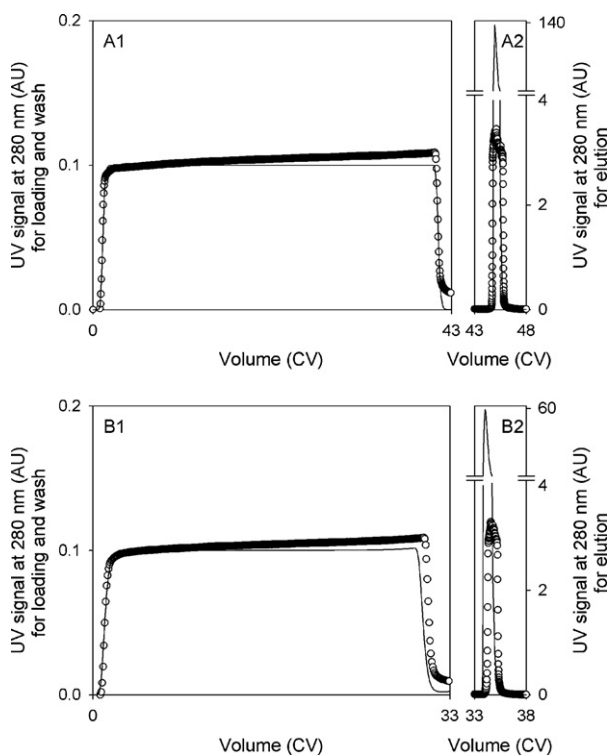


**Fig. 6.** Experimental (○) and simulated (—) breakthrough (left, 1) and desorption (right, 2) curves of  $0.9 \text{ g L}^{-1}$  IgG for AbSolute using a column of  $5 \text{ mm} D \times 50 \text{ mm} L$  with PBS, pH 7.4 (wash), and  $0.1 \text{ M}$  glycine-HCl, pH 3 (elution), as mobile phases flowing at (A)  $200 \text{ cm h}^{-1}$  and (B)  $600 \text{ cm h}^{-1}$  as measured at an absorbance of  $280 \text{ nm}$ . Experimental UV signal > 2 AU is unreliable due to signal saturation.

(total porosity, van Deemter coefficients, apparent friction factor, adsorption isotherm coefficients, and kinetic coefficients) and the corresponding experiments (pulse injections, pressure-flow experiments, and breakthrough experiments) that were performed. A total of approximately 70 person-hours were required for the completion of steps 1 and 2 in Fig. 1. Approximately 80% of this time was spent on the experimentation (step 1) and the remaining 20% on model fitting (step 2). Model validation is usually performed as part of model development to ensure that the model is fit for purpose [6,8–10,12–14]. In this work, however, the model was validated after optimization and not before. This is because process optimization using a lumped parameter model is quick and validating the model at the optimized conditions can reduce the overall experimentation effort, and thus the time and costs, required for the approach. As all the assumptions made during the model development were valid for the experimental data obtained, we proceeded to step 3 with our completed model.

#### 4.2. Model-based process productivity optimization

In this work, productivity,  $PR$ , was optimized mathematically by varying the decision variables on the load, wash and elution volumes ( $V_L$ ,  $V_W$  and  $V_E$ ), at pre-defined column lengths ( $L$ ) and a constant column diameter ( $D$ ) of  $5 \text{ mm}$  based on a feed containing  $1 \text{ g L}^{-1}$  IgG to satisfy a minimum of  $95\%$  yield ( $Y_{\min}$ ) and  $98\%$  purity ( $Pur_{\min}$ ) while operating within a column pressure drop of either  $1.0$  or  $2.5 \text{ bar}$  ( $\Delta P_{\max}$ ) assuming  $24 \text{ h}$  operation. The regeneration and equilibration volumes ( $V_R$  and  $V_Q$ ) were kept constant at  $4 \text{ CV}$  to simplify the optimization problem, as they are practically independent of the flow rates (data not shown). A constant superficial velocity for all the zones (i.e. loading, wash, elution, regeneration and equilibration) was calculated from Eq. (20) based on the maximum column pressure drop,  $\Delta P_{\max}$ , ( $1.0$  or  $2.5 \text{ bar}$ ) and

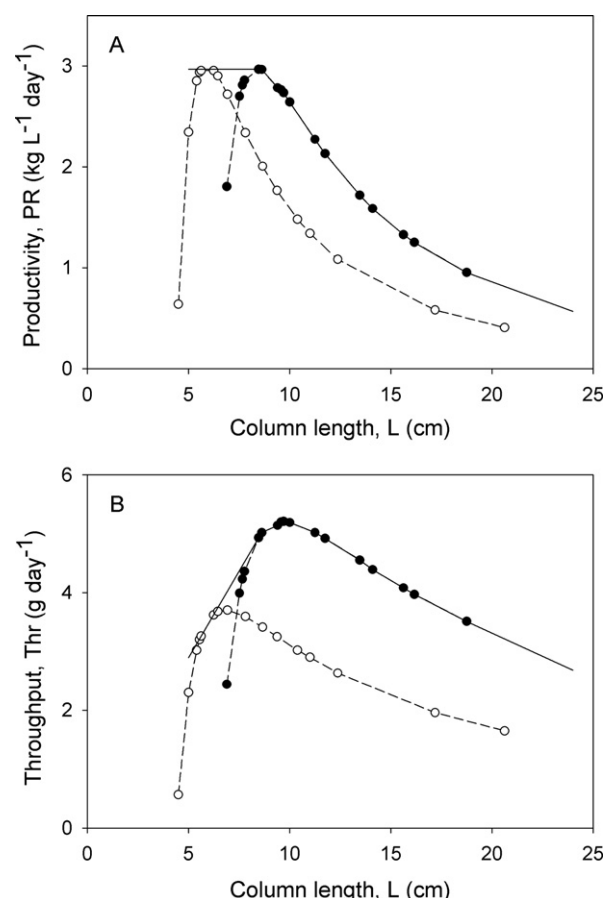


**Fig. 7.** Predicted performance of protein A chromatography for IgG capture by AbSolute, showing (A) productivity and (B) throughput at various column length for a feed containing  $1 \text{ g L}^{-1}$  IgG and a column diameter of  $5 \text{ mm}$  based on  $95\%$  yield and  $98\%$  purity and a maximum column pressure of (○)  $1.0 \text{ bar}$  and (●)  $2.5 \text{ bar}$ .

the estimated apparent friction factor,  $\gamma$ , of  $1.25 \times 10^{-4} \text{ bar h cm}^{-2}$  (Table 3).

The productivity of a batch process based on the lumped parameter model developed earlier was optimized using constrained optimization by linear approximation [23] as described earlier with a precision of  $10^{-6}$ . The optimization was run for different column lengths and the optimum productivity was found for each column length. The optimization problem for each column length was completed in an average of 1 min CPU time on two Intel Xeon E5520 processors of  $2.26 \text{ GHz}$  with  $24.0 \text{ Gb}$  memory.

#### 4.2.1. Optimized batch process conditions

Fig. 7 shows the predicted performance of antibody capture by AbSolute. In the figure, there are clear optimum column lengths for each of the productivity ( $PR$ ) and the corresponding throughput ( $Thr$ ) curves given a particular column pressure drop. At shorter and longer column lengths, limitations are either dominated by kinetics or operational constraints. It is known that IgG breakthrough behavior is effectively identical at constant residence time independent of column dimensions [6,7,10], which is a direct consequence of mass transfer limitations. Considering this and that a shorter column length at a given column pressure drop corresponds to a higher flow rate, i.e. a shorter residence time, it is no surprise that process performance is worse at shorter column lengths. As flow rate decreases with increasing column length, residence time increases and process performance improves as the load approaches the maximum binding capacity. However, flow rate becomes increasingly restricted by the column pressure drop at longer column lengths.

**Table 4**

Batch process operating conditions for IgG capture by AbSolute based on a feed containing  $1 \text{ g L}^{-1}$  IgG for an optimized productivity of  $2.9 \text{ kg L}^{-1} \text{ day}^{-1}$ .

Operating parameter	Symbol	Units	Value
Column length	$L$	mm	85 <sup>a</sup>
Column diameter	$D$	mm	5 <sup>b</sup>
Linear velocity	$u$	$\text{cm h}^{-1}$	2000 <sup>a</sup>
Load volume	$V_L$	CV	15.3 <sup>a</sup>
Wash volume	$V_W$	CV	2.8 <sup>a</sup>
Elution volume	$V_E$	CV	3.3 <sup>a</sup>
Regeneration volume	$V_R$	CV	4.0 <sup>b</sup>
Equilibration volume	$V_Q$	CV	4.0 <sup>b</sup>

<sup>a</sup> Optimized.

<sup>b</sup> Pre-defined.

This significantly lengthens the cycle time and consequently process performance declines.

As can be seen from Fig. 7A, the maximum productivity is  $2.9 \text{ kg L}^{-1} \text{ day}^{-1}$  regardless of the column pressure drop. This corresponds to a column length within the range of 5–8.5 cm, where shorter columns enable operation at lower pressure to achieve the maximum productivity. For example, with a column length of 6 cm the maximum productivity can be achieved at 1.0 bar but not at 2.5 bar due to increased mass transfer limitations from the elevated flow rate. Column lengths shorter than 5 cm were not considered for practical reasons. As for throughput (Fig. 7B), a maximum of  $5.2 \text{ g day}^{-1}$  appears when a column of 5 mm diameter and 10 cm length is operated at 2.5 bar. As expected, the maximum throughput strongly depends on column pressure drop and a much lower value was observed at 1.0 bar. This is because, unlike productivity, throughput is not normalized by the column volume.

Since protein A adsorbents are expensive, the optimum operating conditions (Table 4) were selected based on the maximum productivity for the most economic operation given a maximum column pressure drop of 2.5 bar, which corresponds to the process with a column of 5 mm diameter and 8.5 cm length. A similar productivity can also be achieved with a column of 6 cm length. However, a shorter column length (6 cm versus 8.5 cm) means a wider column diameter (19% increase) given a specific amount of adsorbent to process a particular batch and this can lead to difficulties in column distribution and packing at large scale.

#### 4.3. Model validation with optimized process verification

The process model needs to be validated and it is preferable to verify the optimized batch process experimentally (step 4 in Fig. 1) to ensure that the model is reliable and that the predicted process performance is achievable in practice. This was done by validating the model at the optimum conditions (Table 4) using the same buffers as those used for the breakthrough experiments. The experimental yield and purity were calculated from Eqs. (18) and (19) using the concentrations that were measured by protein A HPLC, which was chosen for analysis for its short analysis time. These experimental values of yield and purity were then compared to the targeted values.

For the example in this work, two separate feeds were considered: human polyclonal IgG, and a model feed of human IgG and bovine serum, each containing  $1 \text{ g L}^{-1}$  IgG. The addition of bovine serum increases the concentration of the impurities, and thus represents a more realistic crude feed providing further challenge to the capture of IgG. The yield and purity obtained for the experimental run with human polyclonal IgG were 99.4% and 99.6%, respectively, whereas those for the experimental run with the model feed were 97.7% and 98.1%, respectively. The constraints of yield (95%) and purity (98%) in the optimization problem were clearly fulfilled by both runs.

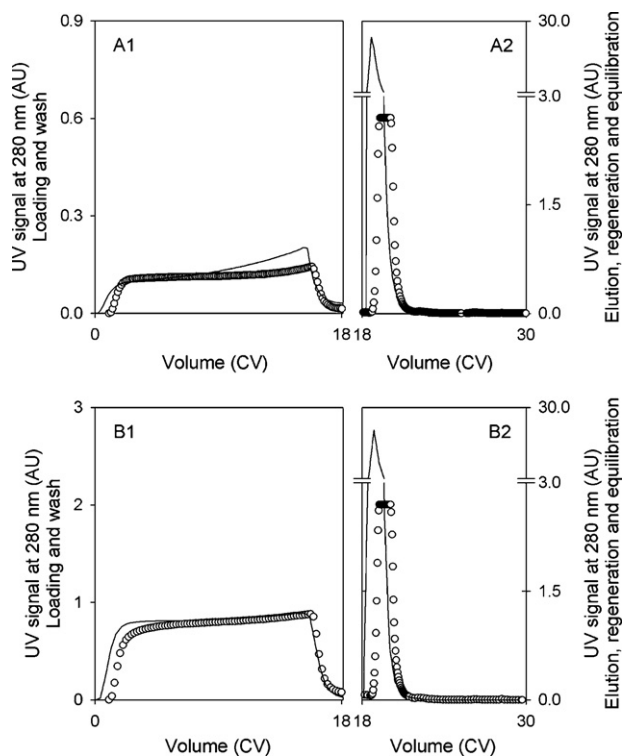


**Fig. 8.** Comparison of (○) experimental and (—) simulated chromatograms for the optimized batch run of IgG capture by AbSolute in a column of  $5 \text{ mm } D \times 85 \text{ mm } L$  based on (A) a feed of human polyclonal IgG, and (B) a model feed of human polyclonal IgG and bovine serum, each containing  $1 \text{ g L}^{-1}$  IgG. Experimental UV signal > 2 AU is unreliable due to signal saturation.

Higher yields were obtained in the experimental batch run than in the simulation. This can be explained by the overestimated IgG breakthrough, i.e. overestimated product loss during loading (Fig. 8). This overestimation could have been anticipated considering the progressively more pessimistic breakthrough prediction with increasing flow in Fig. 5 and the high linear velocity that was optimized for the batch process. This prediction error arose from the high sensitivity of the early breakthrough (around 10%) on the linear velocity, which does not pose a major problem in the current example as it provides added safety to the model and the optimized batch process. If, however, the sensitivity of the early breakthrough on the linear velocity does pose a problem, then an adjustment factor can be added manually to the process conditions by compromising the productivity, e.g. by reducing the load volume by 10%. The adjusted process conditions must be verified experimentally to ensure process feasibility in practice (Fig. 1). Alternatively, an adjustment factor can be added to the model parameters, e.g. to the maximum binding capacity as in [9], before validating the new model using a different set of experimental conditions that was not used for parameter estimation and the initial model validation. Column pressure drop during the experimental batch runs was measured at approximately 2.5 bar, which was around the pre-defined maximum. Therefore, the predicted optimum productivity of  $2.9 \text{ kg L}^{-1} \text{ day}^{-1}$  is feasible for the capture of IgG by AbSolute in practice.

As seen in this work, the optimal operating conditions for the capture of human IgG by AbSolute were identified quickly and accurately using the integrated experimental and modeling approach presented in Fig. 1. Expensive and labor intensive experimentation, and thus time and costs, required for process optimization were drastically reduced by an estimate of two to five folds. The utilization of a lumped parameter model instead of a complex model

reduced the computation time required for optimization, whilst still capturing the main characteristics of the dynamic packed bed behavior and providing the flexibility to incorporate yield and purity constraints into the optimization problem. Based on these results, it can be concluded that the proposed integrated experimental and modeling approach can be very useful for protein A chromatography.

## 5. Conclusion

In this work, an integrated experimental and modeling approach for the design of protein A chromatography for bioprocess manufacture was presented. The approach focuses on the integration of process modeling and experimentation for the design of protein A chromatography as a means to fully exploit the potentials of protein A adsorbents for the capture of antibody in meeting the industry's needs to handle increasing upstream titer and market demand. An integrated approach enables quick, accurate and flexible process optimization, which is otherwise difficult, if not impossible, using a traditional approach based on extensive experimentation. In the integrated approach, small-scale experimentation (step 1 in Fig. 1) is applied to determine the required model parameters (step 2) quickly and inexpensively. The model developed can then be used for model-based process optimization (step 3), the results of which must be verified experimentally to ensure model accuracy and process feasibility in practice (step 4).

The proposed approach was demonstrated through an example of the capture of IgG by a novel silica-based high performance protein A adsorbent called AbSolute. In the example, a transport-dispersive model and an optimization strategy based on process productivity were selected. The productivity of AbSolute was optimized at a column length of 8.5 cm based on a maximum column pressure drop of 2.5 bar. This result was verified experimentally and high performance of  $2.9 \text{ kg L}^{-1} \text{ day}^{-1}$ , 97.7% yield and 98.1% purity were found for the capture of human IgG (from a model feed of  $0.93 \text{ g L}^{-1}$  human polyclonal IgG and 1.1% (v/v) bovine serum containing  $1 \text{ g L}^{-1}$  IgG) by AbSolute in a column of 5 mm diameter and 8.5 cm length.

Overall, the proposed approach enabled the capture of antibody by AbSolute in a batch column to be optimized in 75 person-hours. This illustrates the ease and accuracy of the proposed approach in facilitating the process design of protein A chromatography during process development of bioprocess manufacture. The approach is general and therefore also applicable for other chromatographic processes although the chromatography model and optimization strategy may then differ from those that have been used in the example in this work. For example, the optimization strategy can be improved by varying the loading and elution flow rates from those of the other zones (i.e. wash, regeneration and equilibration) for greater process flexibility, e.g. to cope with kinetics and viscosity differences between zones.

## Nomenclature

$A$	van Deemter eddy diffusion coefficient
$B$	van Deemter mass transfer resistance coefficient ( $\text{s cm}^{-1}$ )
$C$	solute concentration in the mobile phase ( $\text{g L}^{-1}$ )
$C_E$	eluted product concentration ( $\text{g L}^{-1}$ )
$C_f$	feed concentration ( $\text{g L}^{-1}$ )
$C_{\text{IgG}}$	IgG concentration in the mobile phase ( $\text{g L}^{-1}$ )
$C_{\text{imp}}$	impurity concentration in the mobile phase ( $\text{g L}^{-1}$ )
$C_L$	loaded product concentration ( $\text{g L}^{-1}$ )
$C_T$	total eluted concentration ( $\text{g L}^{-1}$ )
$D$	column diameter (cm)

$D_L$	apparent axial dispersion coefficient ( $\text{cm}^2 \text{ s}^{-1}$ )
$d_p$	particle diameter ( $\mu\text{m}$ )
$H$	linear isotherm constant
$h$	reduced plate height
$K_A$	association equilibrium constant ( $\text{L g}^{-1}$ )
$k_m$	lumped mass transfer coefficient ( $\text{s}^{-1}$ )
$k_{\max}$	maximum lumped mass transfer coefficient ( $\text{s}^{-1}$ )
$L$	column length (cm)
$N$	theoretical plate number
$n$	pH dependent equilibrium order
$\text{pH}_{\text{ref}}$	reference pH
$PR$	productivity ( $\text{kg L}^{-1} \text{ day}^{-1}$ )
$Pur$	purity
$q$	solute concentration in the stationary phase ( $\text{g L}^{-1}$ )
$q^*$	solute concentration in the stationary phase at equilibrium ( $\text{g L}^{-1}$ )
$q_{\text{IgG}}^*$	IgG concentration in the stationary phase at equilibrium ( $\text{g L}^{-1}$ )
$q_{\text{imp}}^*$	impurity concentration in the stationary phase at equilibrium ( $\text{g L}^{-1}$ )
$q_{\max}$	maximum binding capacity ( $\text{g L}^{-1}$ )
$q_{\max,R}$	maximum binding capacity of all the retained solutes ( $\text{g L}^{-1}$ )
$q_R$	sum of all the retained solute concentrations in the stationary phase ( $\text{g L}^{-1}$ )
$S_1$	saturation dependent kinetic constant
$S_2$	saturation dependent kinetic order
$t$	time coordinate (s)
$t_0$	column dead time (min)
$t_{\text{cyc}}$	cycle time (min)
$Thr$	throughput ( $\text{g day}^{-1}$ )
$t_L$	loading time (min)
$t_R$	retention time (min)
$u$	linear (superficial) velocity ( $\text{cm h}^{-1}$ )
$\ddot{u}$	vector containing the decision variables for optimization
$V_{\text{col}}$	column volume (ml)
$V_E$	elution volume (ml)
$V_L$	load volume (ml)
$V_Q$	equilibration volume (ml)
$V_R$	regeneration volume (ml)
$V_W$	wash volume (ml)
$Y$	yield
$z$	axial coordinate (cm)

### Greek symbols

$\Delta P$	column pressure drop (bar)
$\varepsilon_T$	total porosity
$\gamma$	apparent friction factor ( $\text{bar h cm}^{-2}$ )
$\omega_{1/2}$	peak width at half maximum peak height

## Acknowledgements

The authors acknowledge the financial support from the UK Engineering and Physical Sciences Research Council (EPSRC).

## References

- [1] A.C.A. Roque, C.S.O. Silva, M.A. Taipa, J. Chromatogr. A 1160 (2007) 44.
- [2] A. Shukla, B. Hubbard, T. Tressel, S. Guhan, D. Low, J. Chromatogr. B 848 (2007) 28.
- [3] D. Low, R. O'Leary, N.S. Pujar, J. Chromatogr. B 848 (2007) 48.
- [4] G. Walsh, Nat. Biotechnol. 28 (2010) 917.
- [5] R.L. Fahrner, D.H. Whitney, M. Vanderlaan, G.S. Blank, Biotechnol. Appl. Biochem. 30 (1999) 121.
- [6] J.T. McCue, G. Kemp, D. Low, I. Quiñones-García, J. Chromatogr. A 989 (2003) 139.
- [7] R. Hahn, R. Schlegel, A. Jungbauer, J. Chromatogr. B 790 (2003) 35.

- [8] R. Hahn, P. Bauerhansl, K. Shimahara, C. Wizniewski, A. Tscheliessnig, A. Jungbauer, *J. Chromatogr. A* 1093 (2005) 98.
- [9] H. Bak, O.R.T. Thomas, J. Abildskov, *J. Chromatogr. B* 848 (2007) 131.
- [10] E.X. Perez-Almodovar, G. Carta, *J. Chromatogr. A* 1216 (2009) 8339.
- [11] E.X. Perez-Almodovar, G. Carta, *J. Chromatogr. A* 1216 (2009) 8348.
- [12] D. Karlsson, N. Jakobsson, A. Axelsson, B. Nilsson, *J. Chromatogr. A* 1055 (2004) 29.
- [13] C.A. Orellana, C. Shene, J.A. Asenjo, *Biotechnol. Bioeng.* 104 (2009) 572.
- [14] B.K. Nfor, D.S. Zuluaga, P.J.T. Verheijen, P.D.E.M. Verhaert, L.A.M. van der Wielen, M. Ottens, *Biotechnol. Prog.* 27 (2011) 1629.
- [15] S. Chan, N. Titchener-Hooker, D.G. Bracewell, E. Sørensen, *AIChE J.* 54 (2008) 965.
- [16] G. Guiochon, A. Felinger, D.G. Shirazi, A.M. Katti, *Fundamentals of Preparative and Nonlinear Chromatography*, 2nd ed., Academic Press, San Diego, 2006.
- [17] H.K. Teoh, E. Sørensen, N. Titchener-Hooker, *Chem. Eng. Sci.* 58 (2003) 4145.
- [18] G. Guiochon, B. Lin, *Modeling for Preparative Chromatography*, Academic Press, New York, 2003.
- [19] G. Ströhlein, L. Aumann, M. Mazzotti, M. Morbidelli, *J. Chromatogr. A* 1126 (2006) 338.
- [20] B.A. Finlayson, *Nonlinear Analysis in Chemical Engineering*, McGraw-Hill, Inc., New York, 1980.
- [21] J.V. Villadsen, M.L. Michelsen, *Solution of Differential Equation Models by Polynomial Approximation*, Prentice-Hall, Inc., Englewood Cliffs, NJ, 1978.
- [22] A.C. Hindmarsh, P.N. Brown, K.E. Grant, S.L. Lee, R. Serban, D.E. Shumaker, C.S. Woodward, *ACM Trans. Maths. Softw.* 31 (2005) 363.
- [23] M.J.D. Powell, in: S. Gomez, J.P. Hennart (Eds.), *Advances in Optimization and Numerical Analysis*, Kluwer Academic, Dordrecht, 1994, p. 51.
- [24] S. Flatman, I. Alam, J. Gerard, N. Mussa, *J. Chromatogr. B* 848 (2007) 79.
- [25] K.M. Usher, C.R. Simmons, J.G. Dorsey, *J. Chromatogr. A* 1200 (2008) 122.
- [26] R. Tran, J.R. Joseph, A. Sinclair, D. Bracewell, Y. Zhou, N.J. Titchener-Hooker, *Biotechnol. Prog.* 23 (2007) 413.
- [27] A. Seidel-Morgenstern, *J. Chromatogr. A* 1037 (2004) 255.
- [28] F. Gritti, G. Guiochon, *J. Chromatogr. A* 1097 (2005) 98.